DOI: 10.7343/as-2018-361

Multi-scenario numerical modeling applied to groundwater contamination: the Popoli Gorges complex aquifer case study (Central Italy)

Modellazione numerica multi-scenario applicata alla contaminazione delle acque sotterrane: il caso dell'acquifero complesso delle Gole di Popoli (Italia centrale)

Diego Di Curzio, Sergio Rusi, Ron Semeraro

Riassunto: In questo lavoro, è stato implementato un modello numerico multi-scenario per esplorare gli effetti della variazione del regime degli emungimenti di un acquifero, sia dal punto di vista idrodinamico, che da quello del trasporto advettivo di contaminanti. Alla fase di implementazione e calibrazione del modello in condizioni stazionarie utilizzando MODFLOW-2005, è seguita la fase di simulazione di diversi scenari di emungimento tra cui lo spegnimento del campo pozzi. I risultati sono stati analizzati attraverso i post processori ZONEBUDGET e MODPATH rispettivamente per valutare il ruolo di ciascuno contributo idrico al bilancio totale e il trasporto advettivo del contaminante.
Le simulazioni hanno evidenziato che allo spegnimento del campo pozzi, finendo l'effetto di barriera idraulica, si ha un aumento del tempo di residenza dei contaminanti e una diminuzione della mobilità nell'acquifero. Inoltre, la diminuzione dell'emungimento causa anche un incremento della portata fluviale, a sua volta responsabile della diluizione della contaminazione nelle acque superficiali.

Keywords: *groundwater, numerical modeling, complex aquifer, advective transport, Popoli Gorges.*

Parole chiave: acque sotterranee, modellazione numerica, acquifero complesso, trasporto advettivo, Gole di Popoli.

Abstract: *In this research, a multi-scenario numerical modeling was implemented to assess the effects of changes to abstraction patterns in the Sant'Angelo well-field (central Italy) and their implications on the aquifer hydrodynamic and the advective transport of contaminants. Once implemented and calibrated the steady-state numerical model by means of MODFLOW-2005, the well-field turning off scenario was modelled. In addition, the numerical results were analyzed by means of the post-processors ZONEBUDGET and MODPATH, to assess respectively the contribution of each hydrogeological feature to the total budget and the advective transport of contaminant particles.*
Comparing the two steady-state numerical models and the relative particle tracking analyses, the well-field turning off, although no longer acting as a hydraulic barrier, increased the residence time of contaminant particles and limited their mobility in the aquifer. Furthermore, the general decrease in groundwater abstractions also caused a higher increase in river flow, favoring contaminants' dilution in surface water.

Introduction

The numerical modeling is widely applied to groundwater management issue which span from assessment of environmental sustainability from abstraction, pumping performance and groundwater storage and recharge (Ayvaz and Karahan 2008; Shammas 2008; Rossetto et al. 2018; Stefania et al. 2018).

Other applications of numerical modelling include the validation of conceptual models for a given hydrogeological context (Rojas et al. 2008; La Vigna et al. 2014; Caschetto et al. 2016; Viaroli et al. 2018a), which improves the understanding of the aquifer system.

Numerical modelling of contaminant fate and transport in groundwater is not of least importance (Greskowiak et al. 2006; Mastrocicco et al. 2012; Refsgaard et al. 2012). Such studies aim to study the evolution of groundwater contamination in the subsurface and support the planning of remedial actions as well as assessing the success of such interventions.

The transport of contaminants in aquifers is widely covered in literature (Freeze and Cherry 1979; Beretta 1992; Fetter 2000; Appelo and Postma 2005) and is connected to several hydrodynamic and hydrogeochemical factors. Most of the factors affecting the movement of contaminants in groundwater tend to slow the downstream movement of the contaminant except for advection, which is directly related to

Diego DI CURZIO
Engineering and Geology Department
University "G. d'Annunzio" of Chieti-Pescara, Pescara, Italy
diego.dicurzio@unich.it

Sergio RUSI
Ron SEMERARO
Engineering and Geology Department
University "G. d'Annunzio" of Chieti-Pescara, Pescara, Italy
s.rusi@unich.it
ronsemeraro@gmail.com

Ricevuto/*Received*: 15 November 2018-Accettato/*Accepted*: 10 December 2018
Pubblicato online/*Published online*: 19 December 2018

the aquifer velocity. Advective transport is clearly related to changes in the hydrodynamics of the aquifer which, in turn, are influenced by changes in the abstraction patterns.

The main objective of this study is to assess the effects of changes to abstraction patterns, which occurred between 2007 and 2008, to the advective transport of groundwater contaminants within an aquifer contaminated with organo-chlorates. The validation of the hydrogeological conceptual model was also a critical objective of the study. A simplified approach was adopted: two scenarios with different boundary conditions (steady-state models) were compared. The simplified approach provides important indications on the contamination spread in the aquifer, mainly because the advective transport influences the downstream movement of a contaminant. Therefore, considerations made in this study can be extended to other cases of groundwater contamination.

Study area

The study area coincides with the Popoli Gorges (PG) at the confluence between the Pescara River and the Tirino River (Central-Eastern Apennines; Fig. 1). There is a significant anthropogenic influence in the area given its strategic location. Critical traffic routes, a hydroelectric plant, a well field (i.e. the Sant'Angelo well field, SAWF) and a chemical industrial site (i.e. the Bussi Officine site, BOS), now no longer active, are all located in the area. Industrial wastes from the latter chemical industrial site were buried near the Pescara River and have now contaminated the groundwater in the area (Di Molfetta & Fracassi 2008; Filippini et al. 2018). Due to this contamination, the well field (approximately 300 l/s; Rusi 2007) was turned off in 2008 and the PG were declared a Site of National Interest (SNI).

Geologically, the area is characterized by a deeply incised riverine valley, which has cut through the Morrone limestone massif. The valley was subsequently filled with quaternary heterogeneous continental deposits (Massoli-Novelli et al. 1998; Conese et al 2001; ISPRA 2006a, 2006b). The Morrone massif is a limestone structure (Triassic-Miocene), mainly limestone or grain supported facies, that overlies more recent clayey-marly formations due to a NW-SE thrust (Conese et al. 2001; ISPRA 2006a, 2006b). Distensive tectonic structures are also present with a NW-SE trend. These structures run below the continental deposits in the PG and disarticulate the limestone massif.

The quaternary continental deposits have a thickness that varies between 65-100 m. These lithologies are variable in nature, depending on the depositional environment (Di Curzio et al. 2016; Vessia and Di Curzio 2018). Specifically, coarse head deposits (i.e. breccias, locally cemented) have been identified. These are associated with the erosion of the limestone massifs in the area and lie on the limestone and clayey-marly bedrock formations. Different travertine facies are found lying over the head deposits. These vary from solid concretions of travertine with cavities to travertine sands. In the western areas, the travertine deposits are incised and infilled with silty-sandy lacustrine deposits and peat, which are locally more clayey. Alluvial deposits are present with discontinuity at the surface across the whole study area. Each geological body present in PG represents a hydrogeological complex of the corresponding aquifer.

Previous studies (Boni et al. 1986; Massoli-Novelli et al. 1998; Conese et al. 2001; Rusi, 2007; Petitta et al. 2018) have identified that groundwater circulation occurs mainly in the continental deposits. The recharge to these

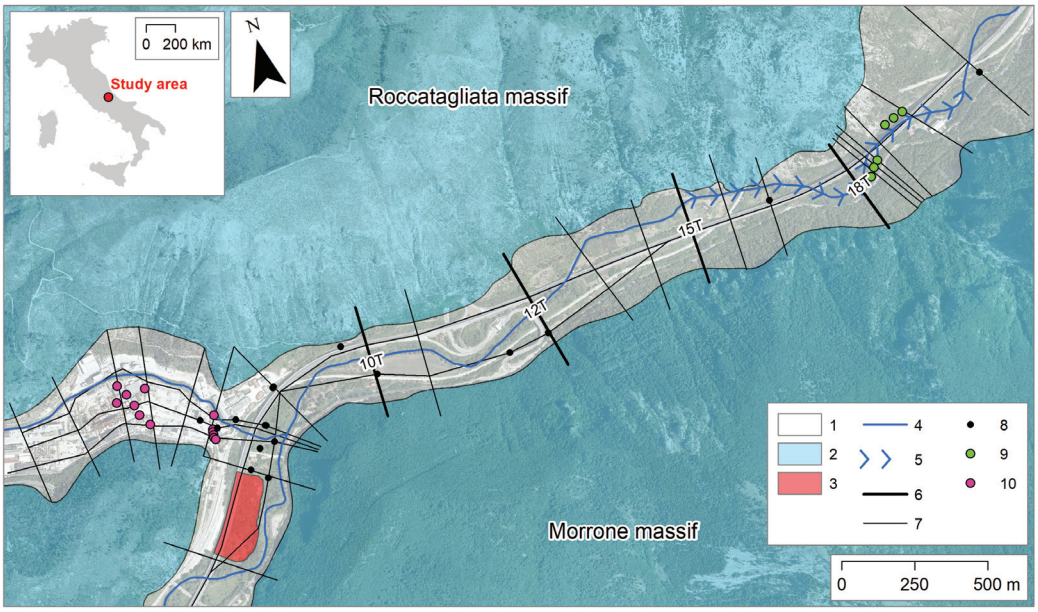

Fig. 1 - Schematic hydro-geological map of the Popoli Gorges. 1) continental deposits; 2) limestone; 3) industrial wastes dump; 4) main rivers; 5) increase in river flow; 6) geological cross-sections shown in the text; 7) hydrogeological cross-sections; 8) piezometers; 9) wells of the SAWF; 10) wells of the hydraulic barriers in the SNI.

Fig. 1 - Carta idro-geologica schematica delle Gole di Popoli. 1) depositi continentali; 2) calcari e calcareniti; 3) Interramento di scarti industriali; 4) fiumi principali; 5) Incremento di portata in alveo; 6) tracce delle sezioni rappresentate nelle immagini del testo; 7) tracce delle sezioni idro-geologiche ricostruite; 8) piezometri; 9) pozzi del SAWF; 10) pozzi delle barriere idrauliche nel SIN.

continental deposits is primarily from the limestone massif and subsequently from rainfall recharge. Surface water-groundwater interactions are known to occur between the Pescara River and the aquifer (Chiaudani et al. 2017). In fact, strong flow increases are observed near SAWF (Fig. 1). This increase in flows has been estimated to be between 0.6 and 1 m^3/s (Boni et al. 1986; Massoli-Novelli et al. 1998; Conese et al. 2001; Rusi 2007). Periodic monitoring of groundwater levels in the area of confluence between Pescara River and the Tirino River (Di Curzio et al. 2014) has identified that changes in groundwater levels correlate with changes in river levels, especially during high flow events.

Dataset

The geometries of the geological bodies that constitute the aquifer were identified through the detailed hydrogeological characterization discussed in Di Curzio et al (2014). This represents the starting point for implementing the numerical model. 32 hydrogeological cross-sections (Fig. 1) were developed utilizing available geological surveys (i.e. borehole logging) and geophysical surveys (i.e. geoelectrical surveys). These were undertaken by Autostrade S.p.A. during the construction of the Pescara-Roma motorway and by ACA S.p.A. for the development of the SAWF. Surveys from ARTA ("Agenzia Regionale per la Tutela dell'Ambiente"; the Regional Environmental Protection Agency) of Abruzzo Region for groundwater monitoring, following the identification of contamination, were also sourced. Survey results from all those companies that have had their activities in the industrial area were also used for the development of the hydrogeological sections.

Groundwater level data used for model calibration purposes were from the monitoring undertaken during the summer of 2007 (Rusi 2007; Di Molfetta and Fracassi 2008). Data from the "Popoli" rain gauge and the "Pescara at Maraone" hydrometric station, located just upstream of the study area, were used to derive respectively the recharge data (model input) and relationships for surface water-groundwater interaction.

Spring discharges available from literature (Boni et al. 1986; Massoli-Novelli et al. 1998; Conese et al. 2001) were used for the water balance outputs. Abstraction data from the SAWF and from the hydraulic barriers developed in the industrial areas were also used as outputs (Rusi 2007; Di Molfetta and Fracassi 2008).

Topography (e.g. stream bed elevation) was implemented in the model using DTM LiDAR 1x1 m data for the Abruzzo Region, provided by the Ministero dell'Ambiente e della Tutela del Territorio e del Mare (MATTM) and distributed under Creative Commons licence.

From the conceptual model to the numerical model (methods)

Steady-state simulations were undertaken to refine the hydrogeological characteristics of the area and to validate the conceptual model. Boundary conditions were subsequently changed to assess the effects of the SAWF turning off.

The numerical model was developed utilizing the MODFLOW-2005 finite difference code (Harbaugh 2005), and the Visual MODFLOW Flex 4.1 graphical user interface. The conceptual model was developed into a numerical model in different phases, as summarized in Fig. 2 for one of the 32 hydrogeological sections.

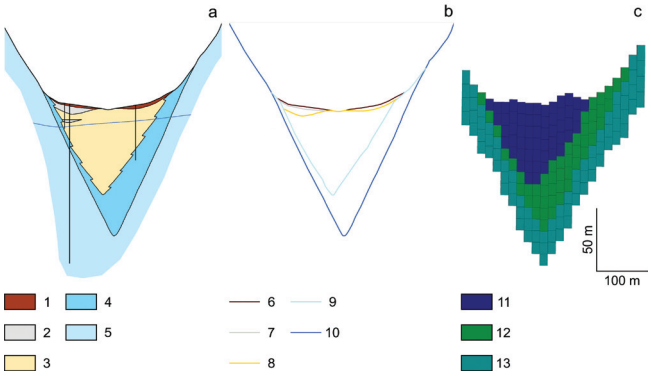

Fig. 2 - Process used to move from the conceptual model to the numerical model: a) hydrogeological cross-section 12T; b) the vectorization of the top of the geological formation; c) model grid. Legend: 1) soil and/or artificial ground; 2) lacustrine deposits; 3) travertine deposits; 4) head deposits; 5) limestone bedrock; 6) top of the soil/artificial ground; 7) top of the lake deposits; 8) top of the travertine deposits; 9) top of the head deposits; 10) top of the bedrock; 11) Zone 2 (travertine deposits); 12) Zone 3 (head deposits); 13) Zone 4 (weathered limestone). Trace of the cross-section in Fig. 1.

Fig. 2 - Conversione dal modello concettuale al modello numerico: a) sezione idrogeologica 12T; b) superfici vettorializzate del top delle formazioni geologiche; c) griglia del modello. Legenda: 1) suolo e/o riporto; 2) depositi lacustri; 3) depositi travertinosi; 4) depositi detritici di versante; 5) substrato calcareo; 6) top del suolo e/o riporto; 7) top dei depositi lacustri; 8) top dei depositi travertinosi; 9) top dei depositi detritici di versante; 10) top del substrato; 11) Zona 2 (depositi travertinosi); 12) Zona 3 (depositi detritici di versante); 13) Zona 4 (calcari fratturati e alterati). Traccia della sezione in Fig. 1.

The hydrogeological sections developed from Di Curzio et al (2014) were first digitized in vectorial format, then imported and georeferenced within the MOVE Midland Valley software. Subsequently, the tops of the different geological formations were digitized. Some geological bodies have limited thickness and lateral extension from a hydrogeological point of view (e.g. soil). These were included in larger hydrogeological bodies with similar hydrogeological properties. To digitalize the top of the geological bodies, Inverse Distance Weighted (IDW) interpolation was used within MOVE to construct the surfaces, then processed within Visual MODFLOW Flex in order to derive the volumetric extension of the geological bodies (Fig. 3) and the subsequent volumetric gridding of the various model layers (Fig. 2c and 4).

A semi-uniform grid was adopted to obtain a discretization that would be representative of the complex geology of the area. Such a grid allows representing complex geometries like pinch-outs, erosive truncation of geological bodies and general lateral discontinuities and changes in lithologies. The layers that result from such a gridding process have variable thickness that are a function of the hydrogeological units represented in the model. The grid is made of 15 layers with variable thickness (Fig. 2c e 4). Each layer has cells of constant 15x15 m dimensions. Each of them was automatically assigned

DOI: 10.7343/as-2018-361

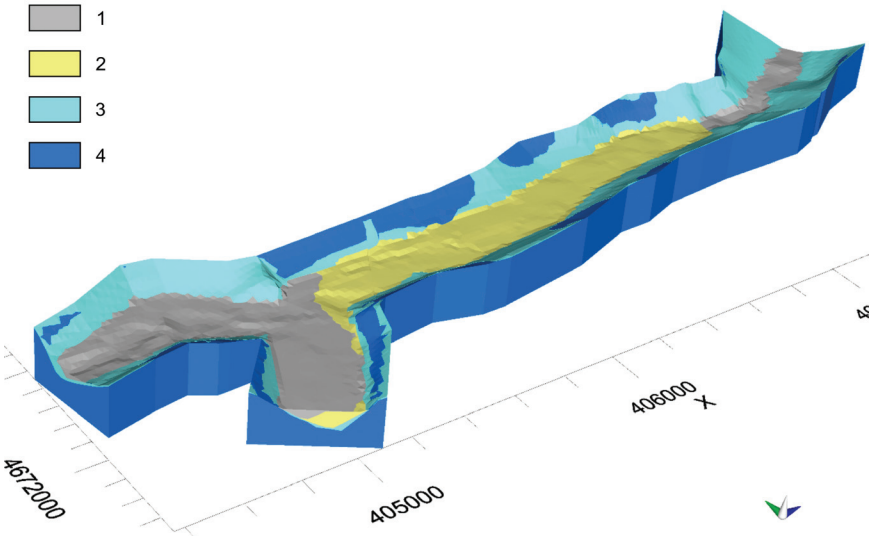

Fig. 3 - 3-D representation of some of the geological bodies present derived from the vectorization of the hydrogeological sections. 1) lacustrine deposits; 2) travertine deposits; 3) head deposits; 4) bedrock.

Fig. 3 - Rappresentazione 3-D di alcuni dei corpi geologici presenti, derivante dalla vettorializzazione delle sezioni idrogeologiche. 1) depositi lacustri; 2) depositi travertinosi; 3) depositi detritici di versante; 4) substrato.

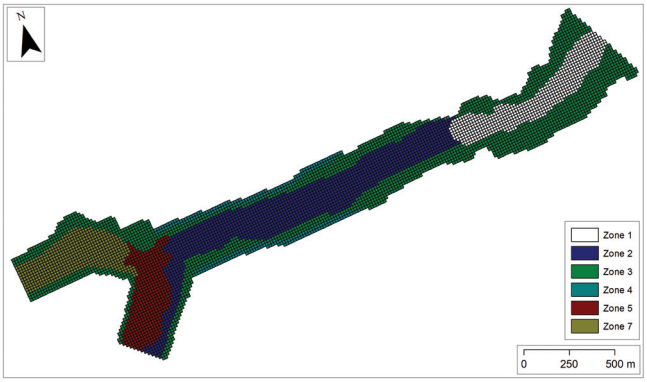

Fig. 4 - Plan showing the different zones of the model (Tab. 1). Zone 6 does not show on the outcrop.

Fig. 4 - Planimetria delle Zone del modello (Tab. 1). La Zona 6 non è presente in affioramento.

Tab. 1 - List of hydrogeological complex present and their respective property zone of the active grid. The hydraulic conductivity values (K_x, K_y, K_z) are in m/s; the effective porosity (n_e) is dimensionless.

Tab. 1 - Elenco dei complessi idrogeologici presenti e relative zone della griglia attiva. I valori di conducibilità idraulica (K_x, K_y, K_z) sono in m/s; la porosità efficace (n_e) è adimensionale.

Hydrogeological complex	Zone	K_x=K_y	K_z	n_e
Alluvial deposits (near the SAWF)	1	$1.0x10^{-4}$	$1.0x10^{-5}$	0.25
Travertine deposits	2	$5.0x10^{-3}$	$5.0x10^{-4}$	0.30
Head deposits	3	$8.0x10^{-3}$	$8.0x10^{-4}$	0.30
Weathered limestone	4	$8.0x10^{-3}$	$8.0x10^{-4}$	0.20
Lacustrine deposits (near the BOS)	5	$6.5x10^{-6}$	$6.5x10^{-7}$	0.12
Lacustrine deposits (near the SAWF)	6	$3.0x10^{-6}$	$3.0x10^{-7}$	0.12
Alluvial deposits (near the BOS)	7	$5.0x10^{-4}$	$5.0x10^{-5}$	0.20

to a specific property zone to permit a more efficient model simulation (Fig. 4).

Hydrogeological parameters were assigned to each property zone (Tab. 1). Specifically, horizontal hydraulic conductivity (K_x and K_y), vertical conductivity (K_z) and effective porosity (n_e) were assigned. These are all necessary with steady-state numerical modelling and particle tracking procedures undertaken with the MODPATH post-processor (Pollock 2012). Initial horizontal hydraulic conductivity values were taken from literature (Rusi 2007, 2014; Gargini et al. 2015) and were optimized during the calibration phase, where horizontal isotropy was chosen (K_x=K_y). An anisotropy ratio K_x/K_z equal to 10 was selected for the vertical conductivity, as suggested by Todd and Mays (2005). Effective porosity values (n_e) were obtained from Singhal and Gupta (2010).

The boundary conditions (Fig. 5) were set after defining the grid and the hydraulic properties of the various zones, attempting to represent the system as realistically as possible. Each hydrogeological element was simulated using different boundary conditions:

- General Head Boundary (GHB) conditions were adopted using hydraulic head distributions taken from literature (Boni et al. 1986; Massoli-Novelli et al. 1998; Conese et al. 2001; Rusi 2007; Desiderio et al. 2012) and the optimized hydraulic conductivity of corresponding deposits to simulate recharge from the Morrone and Roccatagliata massifs. This boundary condition was used along the boundaries of the active grid, only where the limestone bedrock is present, and both upstream and downstream of the continental deposits.
- River (RIV) boundary conditions, used to simulate river features, that interact with groundwater in different parts of the study area. River sections were divided into various segments to improve the simulation of the surface water-groundwater interactions. Each segment has different properties, including river hydraulic head, elevation of the streambed, thickness and vertical conductivity of the streambed deposits and width of the river. These river

features were chosen calibrating the numerical model.

- Well (WEL) boundary conditions were used to simulate abstraction from boreholes and from the hydraulic barriers. The SAWF boreholes, abstracting 300 l/s, and two pump and treat hydraulic barriers, constituted of a total of 13 boreholes (abstraction rates varying between 0.8 l/s and 1.4 l/s) installed in the BOS, were active during the summer 2007 monitoring campaign. This boundary condition was switched off in the second scenario and simulated the SAWF turning off (-300 l/s) following the identification of groundwater contamination. It is important to highlight that the pumping wells in the SAWF have lengths ranging from 32 m up to 63 m. Their filters start at a depth ranging from 6 m to 31 m and reach the bottom in each well. With this set up, the SAWF wells drain groundwater from alluvial deposits, head deposits and fractured limestone. The corresponding layers are variable, although the pumping wells are always located between the 2nd and the 7th layer.
- Recharge (RCH) boundary conditions were used to simulate rainfall recharge. Recharge was initially estimated from the analysis of 1951-2009 rainfall and temperature time-series using the Thornthwaite and Mather (1957) method and with reference to consolidated estimates from literature (Conese et al 2001; Nanni and Rusi 2003; Viaroli et al. 2018b). A constant recharge of 235 mm/y was applied across the entire model area.

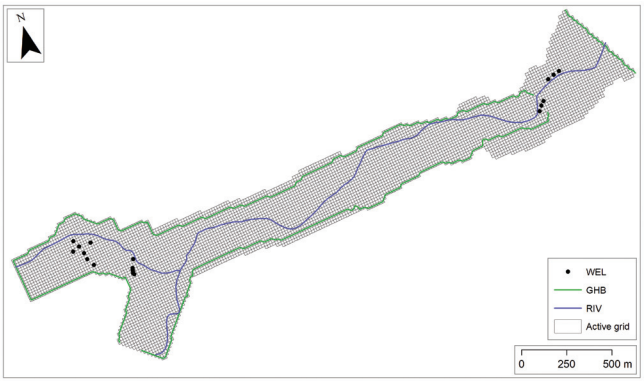

Fig. 5 - Boundary conditions used in the numerical model. The Recharge (RCH) boundary condition was homogeneously applied across the first layer of the grid.

Fig. 5 - Condizioni al contorno adottate nel modello numerico. La condizione al contorno Recharge (RCH) è stata applicata omogeneamente a tutto il primo layer della griglia.

Model calibration

Although the numerical model calibration could be performed automatically by means of specific automated procedures (e.g. PEST; Doherty 2015), at this stage, the Trial & Error approach was chosen. Using this approach, the input parameters must be changed in each model run, until the model results fit the calibration targets. In particular, the calibration targets are the hydraulic heads measured in the monitoring network (Fig. 1), during the summer of 2007. In this model, each calibration target refers to a specific model layer, according with borehole completion depth.

The reliability of the calibration, corresponding to the selected combination of parameters and boundary conditions, was validated using specific criteria and statistics (Wels et al. 2012; Anderson et al. 2015):

- the flow paths and the hydraulic gradients must be comparable with the ones observed in field measurements;
- the Mass Balance Error (MBE) must be less than 1%;
- the Normalized Mean Absolute Error (NMAE) must be less than 10%;
- the Normalized Residual Mean (NRM) must be less than 5%;
- the Normalized Root Mean Square Error (NRMSE) must be less than 10%.

Local water budget

In order to evaluate the specific contribution of each hydrogeological feature to the total budget of the PG aquifer, inflow and/or outflows from the different boundary conditions were calculated by means of ZONEBUDGET (Harbaugh 1990). This MODFLOW post-processor allows to calculate the water budget in every zone of the model domain.

Particle tracking

To evaluate the effects of the SAWF turning off on the advective transport in groundwater, the particle tracking, using MODPATH (Pollock 2012), was performed. The MODPATH post-processor calculates the forward path of each particle and its residence time in the aquifer, starting from hydraulic head and module flux distribution in the numerical domain.

Contamination at the Bussi Officine SNI is mainly related to industrial waste product burials containing chlorinated solvents (Di Molfetta and Fracassi 2008; Filippini et al 2018), that are DNAPLs (Dense Non-Aqueous Phase Liquids). The industrial wastes dump is characterized by a thickness ranging from about 2 m and up to more than 10 m. During the selected time period (i.e. 2007-2008), it was not physically separated from the host rocks, allowing the leaking of chlorinated solvents into the aquifer. These compounds are characterized by low solubility in water and high tendency to be adsorbed on the solid matrix. Furthermore, they move downward into the aquifer, even in the saturated zone, and accumulate at the bottom, releasing slowly chlorinated solvents in groundwater (Beretta 1992; Fetter 1994; Appelo and Postma 2005). In order to reproduce this behavior, the particle starting points were located vertically under the industrial waste dump.

Steady-state numerical model

Below, the results of the numerical model related to summer 2007 monitoring (Scenario 1) are shown, when the SAWF was active. The comparison between simulated and measured hydraulic heads (Fig. 6) and the evaluation statistics (Tab. 2) confirm the hypothesized conceptual model and validate the boundary conditions selected to reproduce every hydrogeological feature of the study area, in

terms of hydraulic conductivity distribution, surface water-groundwater relationships, recharge from the limestone aquifer, groundwater abstractions, and recharge. However, although statistics are always below the suggested thresholds (Tab. 2), sometimes the simulated hydraulic head differs substantially from the measured one (mean error > 1.5 m; Fig. 6). This difference could be ascribable to: i) the intrinsic variability of hydraulic properties within each geological body, especially for coarse head deposits and travertine facies; ii) the lack of accurate information about main rivers, in terms of geometry of river bottom, thickness and hydraulic conductivity of the hyporheic zone, river level distribution within the study area.

Analyzing the numerical modeling results, the hydraulic head distribution (Fig. 8a) related to Scenario 1 suggests that surface water-groundwater interactions exist near the confluence of Pescara and Tirino Rivers. Surface water leaks about 0.107 m^3/s into the aquifer, 0.001 m^3/s of which from Pescara River and 0.106 m^3/s from Tirino River. These results are consistent with the hypothesized conceptual model. In fact, Tirino River recharges the shallower aquifer layers (i.e. alluvial deposits), present beneath the BOS. Instead, Pescara River appears hydraulically connected to groundwater, but it does not leak water into the aquifer.

The surface water-groundwater relationship is reversed near the SAWF. Here, the hydraulic head distribution suggests that groundwater flows into the Pescara River feeding the

Tab. 2 - Evaluation statistical parameters related to the numerical model, compared with the threshold values (Reilly and Harbaugh 2004; Wels et al. 2012; Anderson et al. 2015).

Tab. 2 - Parametri statistici di valutazione del modello numerico calcolati e confrontati con i valori soglia (Reilly & Harbaugh 2004; Wels et al. 2012; Anderson et al. 2015).

Evaluation parameter	Threshold	Calculated value
MBE	< 1%	0.02%
NMAE	< 10%	6.47%
NMR	< 5%	2.33%
NRMSE	< 10%	7.17%

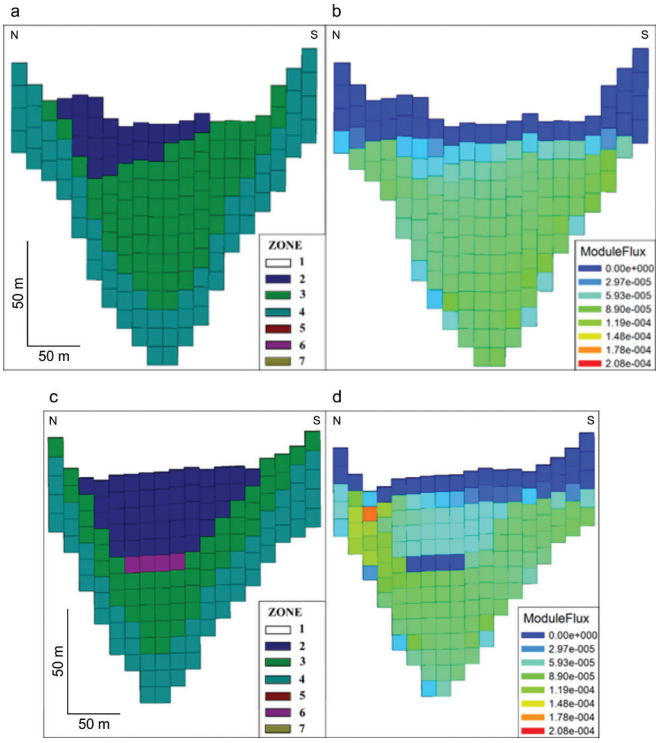

Fig. 7 - Module flux (in m/s) distribution (b and d) within the cross-sections 10T (a) and 15T (c). Traces of the cross-sections in Fig. 1; vertical exaggeration 2x.

Fig. 7 - Distribuzione del flusso modulare in m/s (b e d) in corrispondenza delle sezioni 10T (a) e 15T (c). Tracce delle sezioni in Fig. 1; esagerazione verticale 2x.

increase in river flow reported in literature. Its discharge, calculated in the numerical modeling, is equal to 0.760 m^3/s, as previously measured.

The calculated inflow from the Morrone carbonate aquifer is equal to 0.750 m^3/s. Nevertheless, this inflow seems to be located mainly near the thrust, where the coexistence of a highly fractured rock mass and a groundwater barrier (no flux) facilitate groundwater discharge into the PG aquifer. This is also confirmed by the modeled hydraulic head distribution in the central part of the study area, where, even though the General Head Boundary (GHB) is present, groundwater does

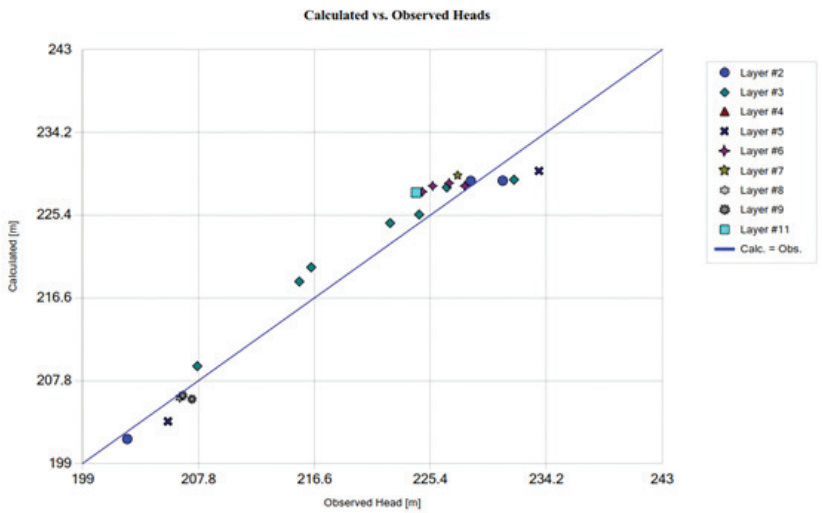

Fig. 6 - Comparison between simulated and measured hydraulic heads (Scenario 1).

Fig. 6 - Confronto tra i carichi idraulici misurati e quelli simulati (Scenario 1).

not seem to interact with the carbonate aquifer.

In addition, the groundwater abstraction effect, from the SAWF and the hydraulic barriers in the BOS, is very clear, since it warps the water table.

As expected in such a heterogenous aquifer, the groundwater flow is not homogeneous. Analyzing the module flux distribution (i.e. the specific discharge in each cell; defined as v = K * i, where K is the hydraulic conductivity and i is the hydraulic gradient) in the cross-sections (Fig. 7), it appears that the module flux is higher within head deposits and weathered bedrock (about $9e^{-5}$ m/s, maximum value about $1.2e^{-4}$ m/s) than within travertine deposits (about $6e^{-5}$ m/s). Lacustrine deposits, instead, show very low module flux values, confirming their role as aquitard. In addition, in Fig. 7d, the very high value (about $1.8e^{-4}$ m/s) refers to the increase in river flow.

Effects of changes to groundwater abstraction pattern

The SAWF turning off has caused significant changes in the PG aquifer hydrodynamic and in the advective transport, whose effects were assessed by means of the numerical modeling. Starting from Scenario 1, groundwater abstraction from the SAWF was excluded (Scenario 2).

Comparing the hydraulic head distributions obtained from the two simulations, differences between the two scenarios are evident, near the SAWF and the increase in river flow. In Scenario 2, the groundwater flow seems to converge more sharply towards the Pescara River than in the Scenario 1. In fact, the discharge of the increase in river flow for Scenario 2 is equal to 0.93 m^3/s (about 22% more than in Scenario 1).

The particle tracking results for the two scenarios (Fig. 8 and 9) show significant differences, especially in the central-eastern part of the study area. Starting from the industrial wastes dump, particles move mostly within the head deposits and the weathered bedrock (Fig. 8a, 8b, 9a and 9b). Near the increase in river flow, most of the particles (66.7%) flows into the Pescara River, in both scenarios (Fig. 8c and 9c, Tab. 3). When the SAWF is active (Scenario 1), the remaining part of the particles flows into the pumping wells (24.4%) and, a lesser part (8.9%), downstream in groundwater (Fig. 8c). In Scenario 2, instead, all the remaining particles (33.3%) flow downstream in groundwater (Fig. 9c).

Tab. 4 shows that the SAWF turning off causes an increase in residence times, especially for minimum values (t_{min} = 106

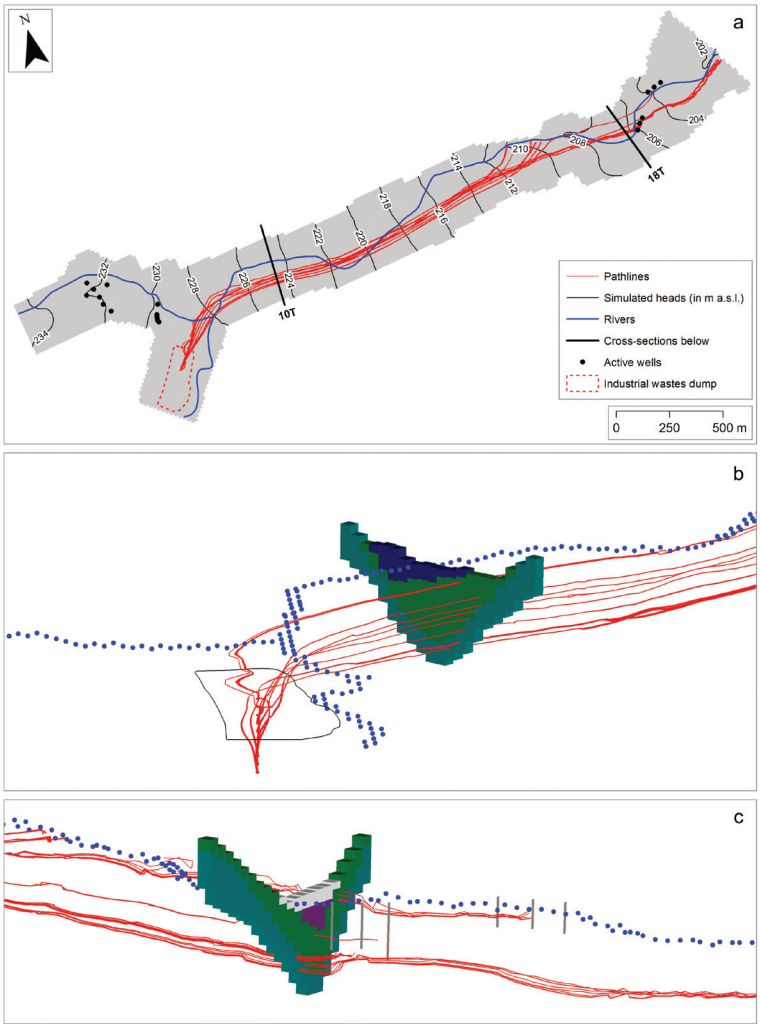

Fig. 8 - Hydraulic head and particle tracking distribution in the Scenario 1 (a). Below: 3-D representation of particle tracking near the cross-sections 10T (b) and 18T (c). Traces of the cross-section in Fig. 1. The blue dots represent the River (RIV) boundary conditions.

Fig. 8 - Distribuzione dei carichi idraulici e dei percorsi delle particelle nello Scenario 1 (a). In basso, distribuzione 3-D delle traiettorie delle particelle, in prossimità delle sezioni 10T (b) e 18T (c). Tracce delle sezioni in Fig. 1. I puntini blu rappresentano le condizioni al contorno di tipo River (RIV).

DOI: 10.7343/as-2018-361

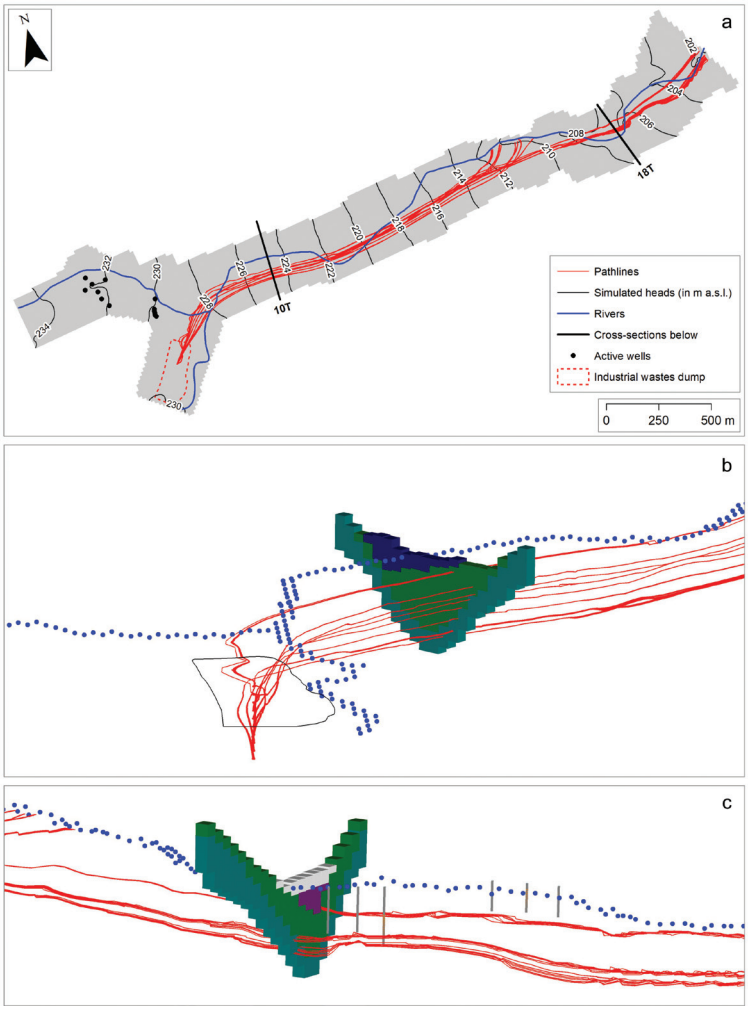

Fig. 9 - Hydraulic head and particle tracking distribution in the Scenario 2 (a). Below, 3-D representation of particle tracking near the cross-sections 10T (b) and 18T (c). Traces of the cross-section in Fig. 1. The blue dots represent the River (RIV) boundary conditions.

Fig. 9 - Distribuzione dei carichi idraulici e dei percorsi delle particelle nello Scenario 2 (a). In basso: distribuzione 3-D delle traiettorie delle particelle, in prossimità delle sezioni 10T (b) e 18T (c). Tracce delle sezioni in Fig. 1. I puntini blu rappresentano le condizioni al contorno di tipo River (RIV).

Tab. 3 - Comparison between particle target percentages in the two scenarios.

Tab. 3 - Confronto tra le percentuali relative ai punti di recapito delle particelle nei due scenari.

Target	% of particles (Scenario 1)	% of particles (Scenario 2)
F. Pescara	66.7	66.7
SAWF	24.4	0
Aquifer downstream	8.9	33.3

Tab. 4 - Comparison between residence times in the two scenarios

Tab. 4 - Confronto tra i tempi di transito nei due scenari.

Travel time	Scenario 1	Scenario 2
t_{max} (days)	1635	1635
t_{min} (days)	107	122
t_{mean} (days)	427	432

days, in Scenario 1; t_{min} = 122 days, in Scenario 2). This effect is clearly related to the substantial groundwater flow decrease (Fig. 10), that takes place as a result of the SAWF turning off. The module flux variation is evident mostly near the SAWF (Fig. 10c and 10d), while it is not significant upstream (Fig. 10a and 10b), near the confluence between the Pescara River and the Tirino River. This suggests that the cone of depression has a relatively small size, although the pumping rate is 300 l/s.

All these differences in hydrodynamic features between the two scenarios have important implications on the advective contaminant transport of the Bussi Officine SNI. In Scenario 1, although the pumping wells of the SAWF act as a hydraulic barrier limiting the contamination spread in groundwater downstream, groundwater abstraction decreases the particle (i.e. contaminants) residence times and facilitate their mobility in the aquifer. On the contrary, in Scenario 2, the decrease in groundwater flow slows down the particle motion in the aquifer, even if the total amount flowing downstream is higher than in Scenario 1. In addition, although the number of particles flowing into the Pescara River is the same in both scenarios (Tab. 3), the higher increase in river flow, caused by the SAWF turning off, favors dilution in surface water, decreasing the contaminants' concentration represented by the particles.

Conclusions and future developments

The hydrogeological modeling results confirmed the great capability of numerical methods in very complex geometry of geological bodies, as in Popoli Gorges.

Useful information could be obtained about the effect of

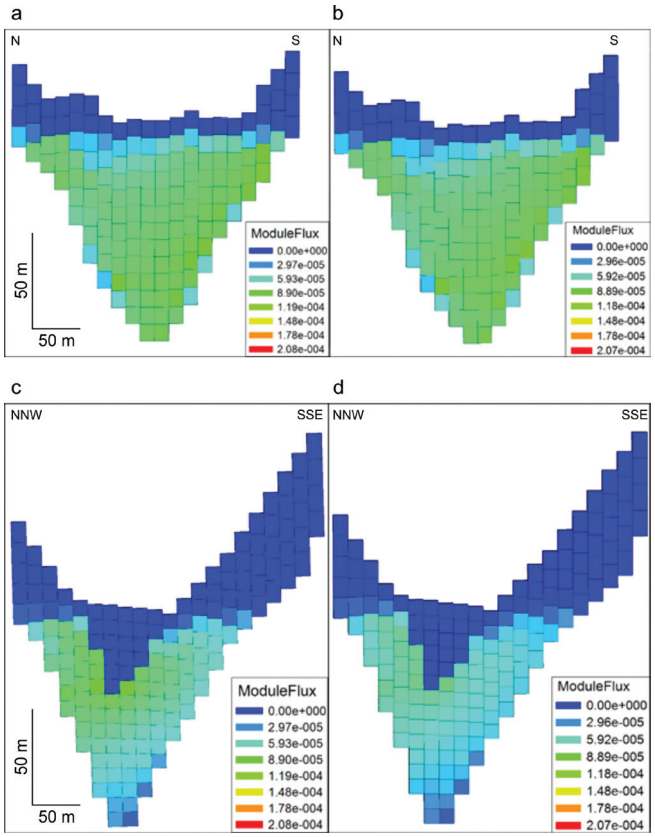

Fig. 10 - Comparison between module fluxes (in m/s) simulated in the Scenarios 1 (a and c) and 2 (b and d), near the cross-sections 10T (above) and 18T (below). Traces of the cross-section in Fig. 1; vertical exaggeration 2x.

Fig. 10 - Confronto tra i flussi modulari (in m/s) negli Scenari 1 (a e c) e 2 (b e d), in corrispondenza delle sezioni 10T (in alto) e 18T (in basso). Tracce delle sezioni in Fig. 1; esagerazione verticale 2x.

the abstraction variations on the aquifer hydrodynamic and the advective contamination transport in groundwater. In fact, the comparison of the two steady-state numerical models and their particle tracking analyses allowed to assess that: 1) the Pescara River is the most important target for the particle that represent in a simplified manner contamination (i.e. only advective transport), regardless of the activity of the well field; 2) the well field, active until 2007, acted as a hydraulic barrier, limiting the contamination spread in groundwater downstream; 3) nevertheless, the cone of depression of the well field decreased the particle (i.e. contaminants) residence times and facilitate their mobility in the aquifer; 4) the well field turning off, although no longer limiting the contamination spread in the aquifer, caused an increase in residence time of particles; 5) the general decrease in groundwater abstractions also caused a higher increase in river flow that favored contaminants' dilution in surface water.

Even though the implemented numerical modeling provided useful information, further developments could be obtained modeling the effect of the wells' turning off on the groundwater contamination by means of an advective-reactive-dispersive transport modeling in transient conditions, that is the next step in this research project.

REFERENCES

Anderson MP, Woessner WW, Hunt RJ (2015) Applied groundwater modeling: simulation of flow and advective transport. Academic press.

Appelo CAJ, Postma D (2005) Geochemistry, Groundwater and Pollution. CRC press.

Ayvaz MT, Karahan H (2008) A simulation/optimization model for the identification of unknown groundwater well locations and pumping rates. Journal of Hydrology 357(1-2):76-92. doi:10.1016/j.jhydrol.2008.05.003

Beretta G P (1992) Idrogeologia per il disinquinamento delle acque sotterranee: tecniche per lo studio e la progettazione degli interventi di prevenzione, controllo, bonifica e recupero *"Hydrogeology for groundwater cleanup: technologies for protection, monitoring, remediation and restoration planning"*. Pitagora Editrice, Bologna.

Boni C, Bono P, Capelli G (1986) Schema Idrogeologico dell'Italia centrale: note illustrative e carte *"Hydrogeological framework of Central Italy: descriptive notes and maps"*. Memorie della Società Geologica Italiana 35:991-1012.

Caschetto M, Colombani N, Mastrocicco M, Petitta M, Aravena R (2016) Estimating groundwater residence time and recharge patterns in a saline coastal aquifer. Hydrological Processes 30(22):4202-4213. doi:10.1002/hyp.10942

Chiaudani, A., Di Curzio, D., Palmucci, W., Pasculli, A., Polemio, M., Rusi, S., 2017. Statistical and fractal approaches on long time-series to surface-water/groundwater relationship assessment: A central Italy alluvial plain case study. Water 9:850. doi:10.3390/w9110850

Conese M, Nanni T, Peila C, Rusi S, Salvati R (2001) Idrogeologia della Montagna del Morrone (Appennino Abruzzese): dati preliminari *"Hydrogeology of the Morrone mountain (Abruzzi, Central Apennines): preliminary data"*. Memorie della Società Geologica Italiana 56:181-196.

Desiderio G, Folchi Vici D'Arcevia C, Nanni T, Rusi S (2012) Hydrogeological mapping of the highly anthropogenically influenced Peligna Valley intramontane basin (Central Italy). Journal of Maps 8(2):165-168. doi:10.1080/17445647.2012.680778

Di Curzio D, Palmucci W, Rusi S (2014) Detailed geological characterization to define groundwater flow in Gole di Popoli (Central Eastern Apennine). Flowpath 2014 - National Meeting on Hydrogeology, Abstract Volume 136-137.

Di Curzio D, Palmucci W, Rusi S., Signanini P (2016) Evaluation of processes controlling Fe and Mn contamination in the San Pedro Sula porous aquifer (North Western Honduras). Rendiconti Online della Società Geologica Italiana 41:42-45. doi:10.3301/ROL.2016.88

Di Molfetta A, Fracassi F (2008) Consulenza tecnica sulla contaminazione in atto nell'area del polo industriale di Bussi *"Technical advice about the ongoing contamination in the Bussi industrial site"*. Consulenza tecnica per conto della Procura della Repubblica presso il Tribunale di Pescara.

Doherty J (2015) Calibration and Uncertainty Analysis for Complex Environmental Models. Watermark Numerical Computing, Brisbane.

Fetter CW (2000) Applied hydrogeology. Prentice-Hall, Englewood Cliffs.

Filippini M, Nijenhuis I, Kümmel S, Chiarini V, Crosta G, Richnow HH, Gargini A (2018) Multi-element compound specific stable isotope analysis of chlorinated aliphatic contaminants derived from chlorinated pitches. Science of The Total Environment, 640:153-162. doi:10.1016/j.scitotenv.2018.05.285

Freeze R, Cherry JA (1979) Groundwater. Prentice-Hall, Englewood Cliffs.

Gargini A, Angeloni A, Crespi D, De Caterini G, De Vita M, Kovacs M, Leoni G, Zaffiro P (2015) Piano della caratterizzazione della discarica abusiva situata in località "I Tre Monti" facente parte del sito di interesse nazionale "Bussi sul Tirino" *Characterizazion plan of the illegal dump in the "I Tre Monti" site belonging to the site of national interest "Bussi sul Tirino"*. Consulenza per conto del Commissario Delegato.

Greskowiak J, Prommer H, Massmann G, Nützmann G (2006) Modeling seasonal redox dynamics and the corresponding fate of the pharmaceutical residue phenazone during artificial recharge of groundwater. Environmental Science & Technology 40:6615-6621. doi:10.1021/es052506t

Harbaugh AW (1990) A computer program for calculating subregional water budgets using results from the USGS modulater 3D finite-difference groundwater flow model. US Geological Survey 24.

Harbaugh AW (2005) MODFLOW-2005, The U.S. Geological Survey Modular Ground-Water Model - the Ground-Water Flow Process. US Geol Surv Tech Methods 253.

ISPRA (2006a) Carta Geologica d'Italia (scala 1:50000), Foglio 360 "Torre de' Passeri" *"Geological map of Italy (1:50000 scale), Section 360 "Torre de' Passeri""*. Servizio Geologico d'Italia.

ISPRA (2006b) Carta Geologica d'Italia (scala 1:50000), Foglio 369 "Sulmona" *"Geological map of Italy (1:50000 scale), Section 369 "Sulmona""*. Servizio Geologico d'Italia.

La Vigna F, Demiray Z, Mazza R (2014) Exploring the use of alternative groundwater models to understand the hydrogeological flow processes in an alluvial context (Tiber River, Rome, Italy). Environmental earth sciences 71(3):1115-1121. doi:10.1007/s12665-013-2515-8

Massoli-Novelli R, Petitta M, Salvati R (1998) La situazione idrogeologica e ambientale delle Gole di Popoli (Abruzzo): primi risultati e prospettive di ricerca *"The hydrogeological and environmental state of the Popoli Gorges (Abruzzi): first results and future research prospectives"*. Memorie della Società Geologica Italiana 53:563-584.

Mastrocicco M, Colombani N, Sbarbati C, Petitta M (2012) Assessing the effect of saltwater intrusion on petroleum hydrocarbons plumes via numerical modelling. Water, Air, & Soil Pollution 223(7):4417-4427. doi:10.1007/s11270-012-1205-6

Nanni T, Rusi S (2003) Idrogeologia del massiccio carbonatico della montagna della Majella (Appennino centrale) *"Hydrogeology of the "montagna della Majella" carbonate massif (Central Apennines-Italy)"*. Bollettino della Società geologica italiana 122(2):173-202.

Petitta M, Mastrorillo L, Preziosi E, Banzato F, Barberio MD, Billi A, Cambi C, De Luca G, Di Carlo G, Di Curzio D et al. (2018) Water-table and discharge changes associated with the 2016-2017 seismic sequence in central Italy: Hydrogeological data and a conceptual model for fractured carbonate aquifers. Hydrogeology Journal 26:1-18. doi:10.1007/s10040-017-1717-7

Pollock DW (2012) User Guide for MODPATH Version 6-A Particle-Tracking Model for MODFLOW. Sect A, Groundw B 6, Model Tech 58 p.

Refsgaard JC, Christensen S, Sonnenborg TO, Seifert D, Højberg AL, Troldborg L (2012) Review of strategies for handling geological uncertainty in groundwater flow and transport modeling. Advances in Water Resources 36:36-50. doi:10.1016/j.advwatres.2011.04.006

Reilly T E, Harbaugh AW (2004) Guidelines for evaluating groundwater flow models. US Department of the Interior, US Geological Survey 30.

Rojas R, Feyen L, Dassargues A (2008) Conceptual model uncertainty in groundwater modeling: Combining generalized likelihood uncertainty estimation and Bayesian model averaging. Water Resources Research 44(12):W12418. doi:10.1029/2008WR006908

Rossetto R, De Filippis G, Borsi I, Foglia L, Cannata M, Criollo R, Vázquez-Suñé E (2018) Integrating free and open source tools and distributed modelling codes in GIS environment for data-based groundwater management. Environmental Modelling & Software 107:210-230. doi:10.1016/j.envsoft.2018.06.007

Rusi S (2007) Studi e ricerche sul comportamento idrodinamico ed idrochimico di acquiferi porosi e fessurati sottoposti ad emungimento a scopo potabile tramite pozzi nelle località di Val Vomano, Pretoro e Castiglione a Casauria gestiti dall'ACA Relazione idrogeologica *"Studies and researches on the hydrodynamic and hydrochemical behavior of porous and fractured aquifers under abstraction conditions for drinking purposes by means of pumping wells in Vomano valley, Pretoro site and Castiglione a Casauria site managed by ACA. Hydrogeological report"*. Report interno ACA (Azienda Consortile Acquedottistica) S.p.A.

Rusi S (2014) Prove di permeabilità sul campo pozzi San Rocco nel comune di Bussi sul Tirino senza interruzione della distribuzione in rete *"Pumping tests in the San Rocco well field in Bussi sul Tirino during water supply"*. Report interno ACA (Azienda Consortile Acquedottistica) Spa.

Shammas MI (2008) The effectiveness of artificial recharge in combating seawater intrusion in Salalah coastal aquifer, Oman. Environmental Geology 55(1):191-204. doi:10.1007/s00254-007-0975-4

Singhal BBS, Gupta RP (2010) Hydraulic Properties of Rocks. In: Applied Hydrogeology of Fractured Rocks. Springer, Dordrecht. doi:10.1007/978-90-481-8799-7_8

Stefania GA, Rotiroti M, Fumagalli L, Simonetto F, Capodaglio P, Zanotti C, Bonomi T (2018) Modeling groundwater/surface-water interactions in an Alpine valley (the Aosta Plain, NW Italy): the effect of groundwater abstraction on surface-water resources. Hydrogeology Journal 26(1):147-162. doi:10.1007/s10040-017-1633-x

Thornwaite CW, Mather JR (1957) Instructions and tables for computing potential evapotranspiration and the water balance. Publications in Climatology 10(3):183-243.

Todd DK, Mays LW (2005) Groundwater hydrology. Wiley, Hoboke.

Vessia G, Di Curzio D (2018) Lacustrine Deposits. In: Bobrowsky P., Marker B. (eds) Encyclopedia of Engineering Geology. Encyclopedia of Earth Sciences Series. Springer, Cham. doi:10.1007/978-3-319-12127-7_179-1

Viaroli S, Lotti F, Mastrorillo L, Paolucci V, Mazza R (2018a) Simplified two-dimensional modelling to constrain the deep groundwater contribution in a complex mineral water mixing area, Riardo Plain, southern Italy. Hydrogeology Journal. doi: 10.1007/s10040-018-1910-3

Viaroli S, Mastrorillo L, Lotti F, Paolucci V, Mazza R (2018b) The groundwater budget: A tool for preliminary estimation of the hydraulic connection between neighboring aquifers. Journal of Hydrology 556:72-86. doi:10.1016/j.jhydrol.2017.10.066

Wels C, Mackie D, Scibek J (2012) Guidelines for groundwater modelling to assess impacts of proposed natural resource development activities. Ministry of Environment, Water Protection & Sustainability Branch.